

## **Electronic Supplementary Information**

# **Enhanced room-temperature NO<sub>2</sub> sensing properties of biomorphic hierarchical mixed phase WO<sub>3</sub>**

He Lv<sup>a</sup>, Zhuo Liu<sup>a</sup>, Junkun Chen<sup>a</sup>, Muhammad Ikram<sup>a</sup>, Xue Bai<sup>a</sup>, Jue Wang, Baihe Sun, Kan Kan<sup>\*b</sup>, and Keying Shi<sup>\*a</sup>

<sup>a</sup> *Key Laboratory of Functional Inorganic Material Chemistry, Ministry of Education. School of Chemistry and Material Science, Heilongjiang University, Harbin, 150080, P. R. China. E-mail: shikeying2008@163.com*

<sup>b</sup> *Heilongjiang Academy of Sciences, Institute of Advanced Technology, Harbin 150020, P. R. China. E-mail:  
kankan.has@foxmail.com*

## Table of contents

- P1 Cover page
- P2 **Table of contents**
- P3 **Table S1** The sensing performance of the single crystal phase  $\text{WO}_3$  for  $\text{NO}_2$  gas sensing
- P4 **Table S2** Comparison of gas sensing performance of the  $\text{WO}_3$  based composite towards  $\text{NO}_2$  gas with previous reported work.
- P5 **Table S3** Previous effort of mixed-phase materials used in different fields.
- P6 **Table S4** Previous effort of bio-template materials used in different fields.
- Table S5** Experimental conditions and crystal type of B- $\text{WO}_3$ -ab and pure  $\text{WO}_3$ -ab materials.
- P7 **Fig. S1**  $I_m$  and  $I_h$  values of hexagonal (JCPDS 33-1387) and monoclinic (JCPDS 72-0677) phases of (a) BC- $\text{WO}_3$ -22, (b) BC- $\text{WO}_3$ -04, and (c) BC- $\text{WO}_3$ -24.
- Fig. S2** Energy-dispersive X-ray spectroscopy (EDS) analysis of (a) B- $\text{WO}_3$ -22, (b) B- $\text{WO}_3$ -04, (c) B- $\text{WO}_3$ -24.
- P8 **Fig. S3** XRD, FTIR and Raman of biomass carbon.
- P9 **Fig. S4** The TEM/HRTEM/SAED pattern images of B- $\text{WO}_3$ -04.
- Fig. S5** The TEM Mapping images of B- $\text{WO}_3$ -04.
- P10 **Fig. S6** Nitrogen adsorption-desorption isotherms of hemp-derived biomass carbon and B- $\text{WO}_3$ -ab.
- Fig. S7** Comparison of the XPS full spectra of B- $\text{WO}_3$ -22, B- $\text{WO}_3$ -04 and B- $\text{WO}_3$ -24.
- Table S6** Contents of C, O, W, and Na in XPS of B- $\text{WO}_3$ -22, B- $\text{WO}_3$ -04 and B- $\text{WO}_3$ -24.
- P11 **Table S7** Response, response time and recovery time of B- $\text{WO}_3$ -22, B- $\text{WO}_3$ -04, and B- $\text{WO}_3$ -24 sensors.
- Fig. S8** Dynamic response-recovery curve of pure  $\text{WO}_3$ -40 and  $\text{WO}_3$ -04.
- Table S8** Response, response time and recovery time of  $\text{WO}_3$ -40 and  $\text{WO}_3$ -04.
- P12 **Fig. S9** Response of the B- $\text{WO}_3$ -04 sensor to 100 ppm  $\text{NO}_2$  as a function of the relative humidity.
- Table S9** Fitted impedance parameters of B- $\text{WO}_3$ -22, B- $\text{WO}_3$ -04, and B- $\text{WO}_3$ -24 samples.
- References**

**Table S1** The sensing performance of the single crystal phase  $\text{WO}_3$  for  $\text{NO}_2$  gas sensing.

Morphology	Crystal type of $\text{WO}_3$	$\text{NO}_2$ (ppm)	Operating temperature (°C)	Response	LOD	Ref.
nanoparticles	hexagonal or monoclinic	5	100	251.7	50 ppb	1
nanotubes	monoclinic	5	300	100.3	>20 ppb	2
nanorods	monoclinic	10	225	2.02	2 ppm	3
nanosheets	Hexagonal or monoclinic	1	100	62.1	100 ppb	4
thin films	monoclinic	5	150	5.75	1 ppm	5
nanoplates	orthorhombic	5	100	10	1 ppm	6
dendrites	hexagonal	5	140	32.9	20 ppb	7
ultrathin nanosheet	monoclinic	50 ppb	140	5.67	10 ppb	8
thin film	monoclinic	200	200	38%	50 ppm	9
flower-like	monoclinic	80 ppb	90	190.8	5 ppb	10
yolk–shell spheres	monoclinic	100 ppb	100-200	120	30 ppb	11
cuboid or hexagonal plate-like	monoclinic or hexagonal	20 ppb 500 ppb	200 200	160 120		12

**Table S2** Comparison of gas sensing performance of the  $\text{WO}_3$  based composite towards  $\text{NO}_2$  gas with previous reported work.

Sensing materials	$\text{NO}_2$ (ppm)	Operating temperature (°C)	Response	$t_{\text{res}}/t_{\text{rec}}$	LOD	Recoverability	Refs.
APTES-functionalized porous $\text{WO}_3$	10	340	184	11s/12s	10 ppb	complete	13
$\text{Au}@\text{WO}_3$	5	100	136	4s/59s	250ppb	complete	14
Sb-doped $\text{WO}_3$	2	70	343	70s/50s	0.5ppm	incomplete	15
Au NP-decorated $\text{WO}_3$	1	150	96	9s/16s	0.6ppm	complete	16
Pd-doped $\text{WO}_3$	5	150	283.96	26s/66s	50ppb	complete	17
$\text{WO}_3/\text{ZnO}$	1	150	168		250ppb	complete	18
Au-doped $\text{WO}_3$	5	175	212.3	10s/120s	50ppb	complete	19
$\text{WO}_3-\text{rGO}$	10	90	4.3	4.1s/5.8s		complete	20
Sb- $\text{WO}_3$	10	RT	51		1ppm	incomplete	21
Bis-crystalline phase $\text{WO}_3$	100	RT	71.07	3s/11.6s	50ppb	complete	Present work

**Table S3** Previous effort of mixed-phase materials used in different fields.

Materials	Synthesis process	Applications	References
2H and 1T mixed phase few-layer MoS <sub>2</sub>	hydrothermal	photocatalytic hydrogen evolution	22
rutile and anatase phase TiO <sub>2</sub>	electrochemical anodization	photocatalytic	23
anatase / rutile phase TiO <sub>2</sub>	electrochemical anodization	photoelectrochemical	24
2H and 1T mixed phase MoS <sub>2</sub>	solution-exfoliated and anneal	hydrogen evolution	25
amorphous/crystalline Ga <sub>2</sub> O <sub>3</sub>	radio frequency(RF) magnetron sputtering growth technique	Solar-Blind Photodetection	26
anatase/rutile/srilankite phase TiO <sub>2</sub>	flame synthesis	photocatalytic hydrogen evolution	27
rhombohedral and tetragonal phase BiFeO <sub>3</sub>	microscopic resistive switching device	epitaxially strained thin film of BFO	28
monoclinic hexagonal phase WO <sub>3</sub>	photocatalytic water splitting	solvothermal	29
rutile/anatase phase TiO <sub>2</sub>	magnetron sputtering deposition	photocatalysts	30
Nb-doped natase and utile phase TiO <sub>2</sub>	deposition	photocatalysts	31
anatase /rutile phase TiO <sub>2</sub>	framework vanadium doping and heat treatments	photocatalysts	32
α-βmixed-phase Ga <sub>2</sub> O <sub>3</sub>	----	photocatalytic water splitting	33
α-δ mixed-phase FAPbI <sub>3</sub>	anneal	near-infrared emission	34

**Table S4** Previous effort of bio-template materials used in different fields.

Biomass Materials	Based Materials	Synthesis process	Applications	Refs.
kiwi peel	NiS <sub>2</sub>	hydrothermal	electro-chemical sensor	34
wood	MnO	hydrothermal	electromagnetic wave absorption	35
absorbent cotton	ZnO	impregnation and calcination	H <sub>2</sub> S gas-sensing	36
enteromorpha prolifera	MoO <sub>3</sub>	freezer drying	glucose colorimetric assay	37
cellulose nanocrystals	WO <sub>3</sub>	electrospinning	H <sub>2</sub> S gas-sensing	38
eucheuma	CdS	freezer drying	photocatalytic hydrogen evolution	39
waste paper pieces	WO <sub>3</sub>	tubular coking furnace	electrochemical materials	40
carrageenan	FeS	calcination in CO <sub>2</sub> atmosphere	sodium-ion batteries	41
seaweed fiber	SnO <sub>2</sub>	wet-spinning	triethylamine detection	42

**Table S5** Experimental conditions and crystal type of B-WO<sub>3</sub>-ab and pure WO<sub>3</sub>-ab materials.

Samples	Time (h)		Crystal type
	350°C	450°C	
B-WO <sub>3</sub> -22	2h	2h	h-WO <sub>3</sub> m-WO <sub>3</sub>
B-WO <sub>3</sub> -04	0h	4h	h-WO <sub>3</sub> m-WO <sub>3</sub>
B-WO <sub>3</sub> -24	2h	4h	h-WO <sub>3</sub> m-WO <sub>3</sub>
WO <sub>3</sub> -40	4h	0h	h-WO <sub>3</sub>
WO <sub>3</sub> -04	0h	4h	m-WO <sub>3</sub>

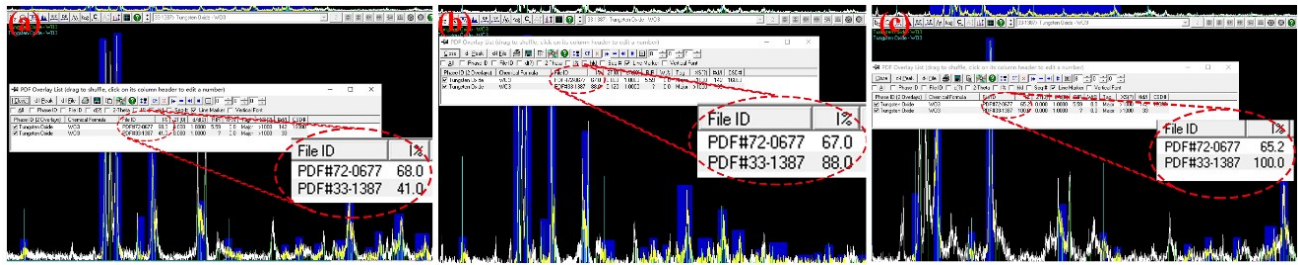


**Fig. S1** I<sub>m</sub> and I<sub>h</sub> values of hexagonal (JCPDS 33-1387) and monoclinic (JCPDS 72-0677) phases of (a) BC-WO<sub>3</sub>-22, (b) BC-WO<sub>3</sub>-04, and (c) BC-WO<sub>3</sub>-24.

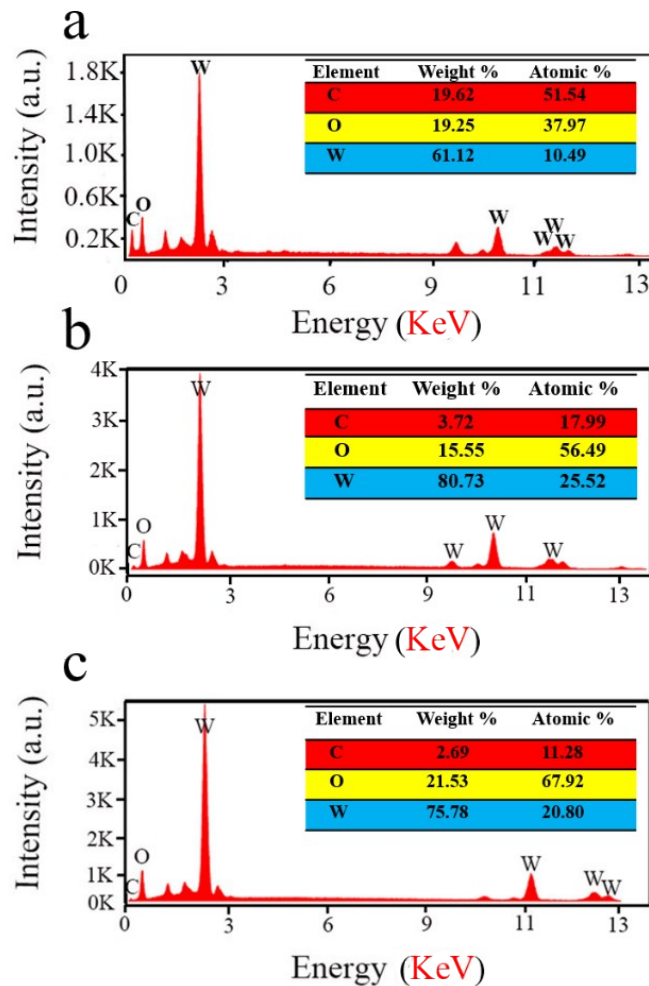


**Fig. S2** Energy-dispersive X-ray spectroscopy (EDS) analysis of (a) B-WO<sub>3</sub>-22, (b) B-WO<sub>3</sub>-04, (c) B-WO<sub>3</sub>-24.

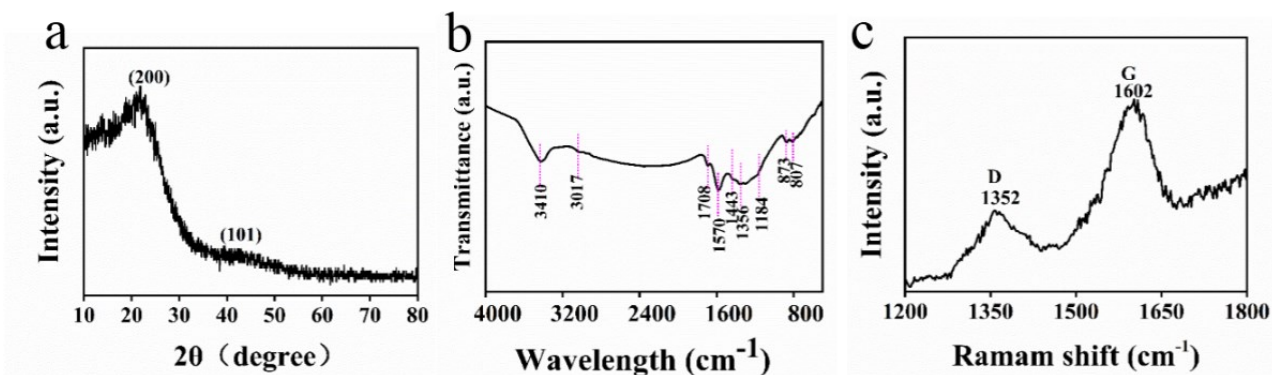


**Fig. S3** XRD, FTIR and Raman of biomass carbon.

Fig. S3a exhibited two broad peaks at around  $22^\circ$  corresponding to the (002) and  $43^\circ$  corresponding to the (100) plane of graphite, suggesting the formation of the carbon product with a limited graphitization degree. Fig. S3b shows a broad absorption bands around  $3410\text{ cm}^{-1}$  is assigned to the stretching vibrations of the O–H groups and the bending vibrations of a small quantity of adsorbed water molecules. And a weak absorbance around  $1708\text{ cm}^{-1}$  in the FTIR spectrum of biomass carbon, which might be attributed to the presence of the carboxylic ester ( $\text{C=O}$ ) in pectin and waxes. The benzene ring and side chain of lignin have the inherent  $\text{C=C}$  bond of biomass and the absorption peak is located at  $1570\text{ cm}^{-1}$ . The carbon material prepared by nitric acid activation has a distinct peak here, indicating that the use of nitric acid can increase  $\text{C=C}$ . The observed peaks at  $1679$  and  $832\text{ cm}^{-1}$ , which are ascribed to a stretching vibration of  $\text{C=O}$  and  $\delta\text{-CH}$ . The bands at about  $1443\text{ cm}^{-1}$  are ascribed to the C–H inplane bending vibration. The presence of C–O bonds in various chemical surroundings have been shown to be within the  $1356\text{--}950\text{ cm}^{-1}$  range. It should be noted that the  $1184\text{ cm}^{-1}$  bands are normally ascribed to O–H bending vibrations.<sup>43–46</sup> The chemical functional group -COOH produced during the strong acid treatment (chemical oxidation) enhanced the hydrophilicity of biomass carbon and improved its dispersibility in the  $\text{WO}_3$  matrix.<sup>47–49</sup>

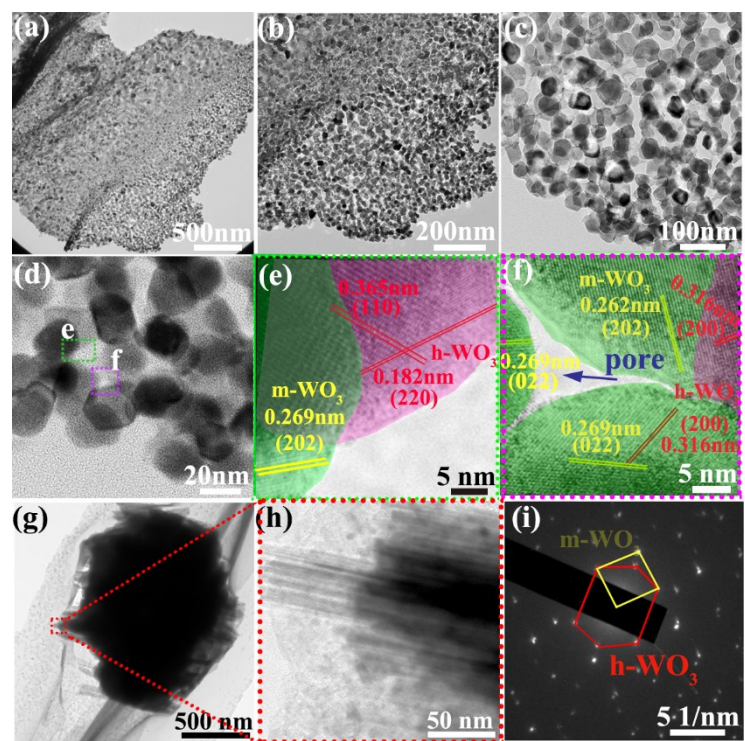


**Fig. S4** The TEM/HRTEM/SAED pattern images of B-WO<sub>3</sub>-04.

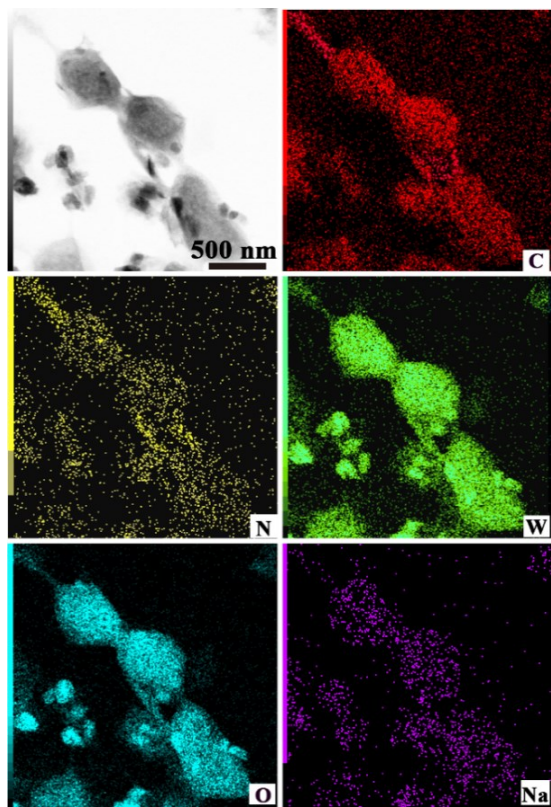


**Fig. S5** The TEM Mapping images of B-WO<sub>3</sub>-04.

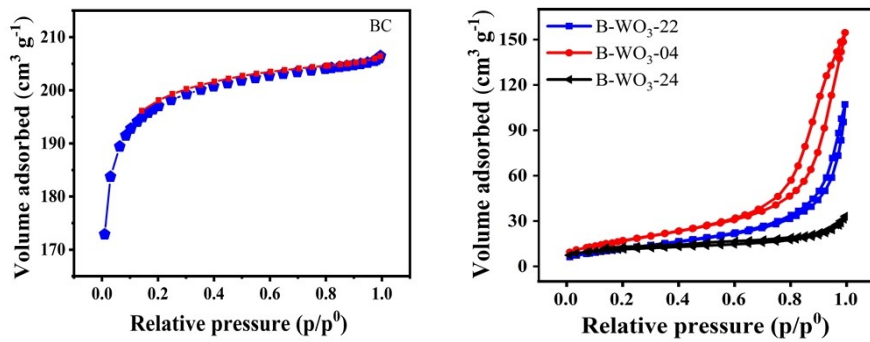


**Fig. S6** Nitrogen adsorption-desorption isotherms of hemp-derived biomass carbon and B-WO<sub>3</sub>-ab.

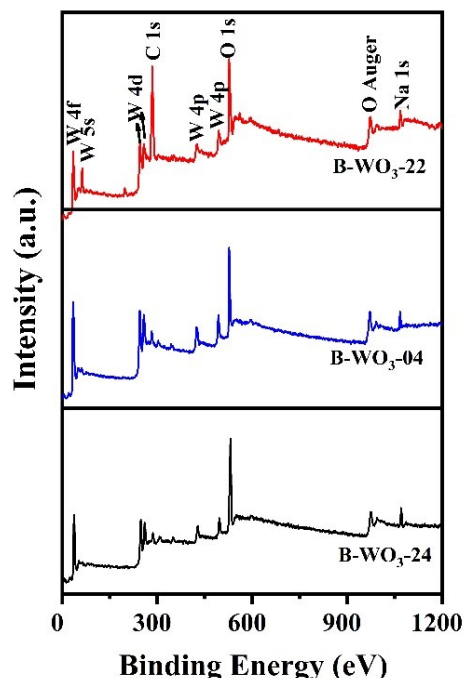


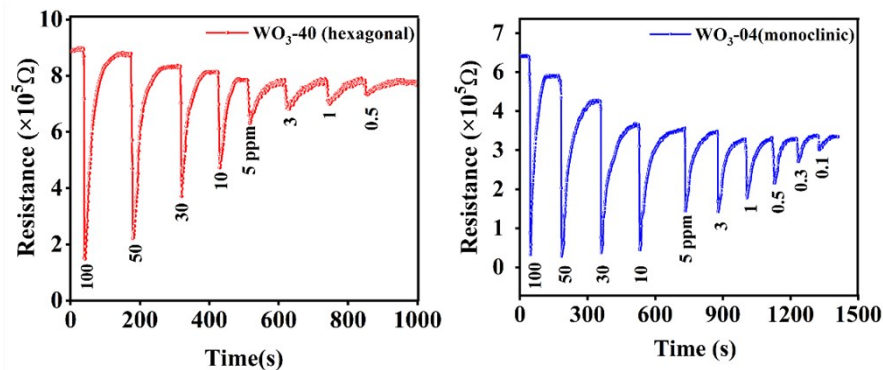
**Fig. S7** Comparison of the XPS full spectra of B-WO<sub>3</sub>-22, B-WO<sub>3</sub>-04 and B-WO<sub>3</sub>-24.

**Table S6** Contents of C, O, W, and Na in XPS of B-WO<sub>3</sub>-22, B-WO<sub>3</sub>-04 and B-WO<sub>3</sub>-24.

Samples	C (at%)	O (at%)	W (at%)	Na (at%)
B-WO <sub>3</sub> -22	55.42	29.81	12.45	2.32
B-WO <sub>3</sub> -04	16.43	52.83	27.23	3.51
B-WO <sub>3</sub> -24	12.66	59.62	23.57	4.15

**Table S7** Response, response time and recovery time of B-WO<sub>3</sub>-22, B-WO<sub>3</sub>-04, and B-WO<sub>3</sub>-24 sensors.

Sensors	B-WO <sub>3</sub> -22			B-WO <sub>3</sub> -04			B-WO <sub>3</sub> -24			
	NO <sub>2</sub> (ppm)	R	T <sub>s</sub>	T <sub>r</sub>	R	T <sub>s</sub>	T <sub>r</sub>	R	T <sub>s</sub>	T <sub>r</sub>
100	57.45	6.40	29.2	71.07	3	11.6	37.52	7.13	36.4	
50	51.72	9.07	37.6	60.09	4.53	21.2	35.45	7.60	46.8	
30	45.52	10.13	53.6	51.09	4.97	22	30.72	8.40	48.8	
10	21.92	11.73	53.2	27.49	6	31.8	22.92	9.13	53.2	
5	16.48	11.27	56	17.29	7.27	32	12.48	9.80	51.2	
3	4.29	11.73	53.2	5.69	7	42.4	4.29	10.07	52.4	
1	2.39	13.87	37.2	2.63	9	46	2.39	11.73	52.8	
0.5	1.98	12.27	37.4	2.52	9.96	48.6	1.98	13.87	67.6	
0.3	1.84	14.27	42.4	2.08	12.8	45.6	1.34	14.27	40.4	
0.1	1.38	15.73	37	1.65	12.27	28.4	1.18	14.80	42.8	
0.05	1.12	16.40	29.2	1.38	11.2	20.8				

\*R: Response    T<sub>s</sub>: Response time    T<sub>r</sub>: Recovery time**Fig. S8** Dynamic response-recovery curve of pure WO<sub>3</sub>-40 and WO<sub>3</sub>-04.**Table S8** Response, response time and recovery time of WO<sub>3</sub>-40 and WO<sub>3</sub>-04.

Sensors	WO <sub>3</sub> -40			WO <sub>3</sub> -04			
	NO <sub>2</sub> (ppm)	R	T <sub>s</sub>	T <sub>r</sub>	R	T <sub>s</sub>	T <sub>r</sub>
100	11.45		10.40	41.2	25.07	12	46.2
50	10.72		10.07	47.6	21.59	14.53	50.6
30	8.52		11.13	53.6	17.09	19.97	53.6
10	6.92		12.73	53.2	8.49	26	63.2
5	5.48		11.27	56	6.29	27.27	69
3	4.29		12.53	53.2	5.69	27	73.2
1	2.09		13.17	37.2	2.63	29	78.2
0.5	1.18		14.57	37.4	2.12	29.96	77.4
0.3					1.68	22.8	71.2
0.1					1.05	22.27	66.8

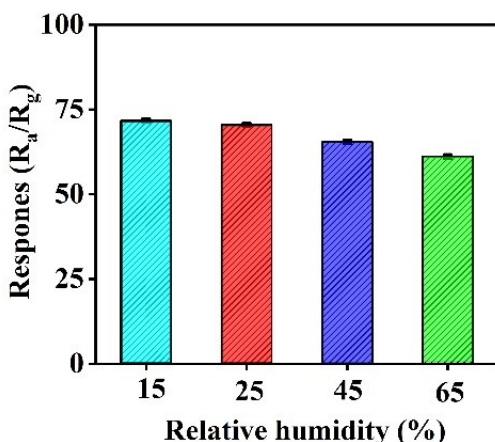


**Fig. S9** Response of the B-WO<sub>3</sub>-04 sensor to 100 ppm NO<sub>2</sub> as a function of the relative humidity.

**Table S9** Fitted impedance parameters of B-WO<sub>3</sub>-22, B-WO<sub>3</sub>-04, and B-WO<sub>3</sub>-24 samples.

Samples	B-WO <sub>3</sub> -22	B-WO <sub>3</sub> -04	B-WO <sub>3</sub> -24
$R_s (\Omega)$	78	58	61
$R_{ct} (\Omega)$	834.9	537.8	691.6

## References

1. T. Li, Y. Shen, S. Zhao, X. Zhong, W. Zhang, C. Han, D. Wei, D. Meng and Y. Ao, Journal of Alloys and Compounds, 2019, 783, 103-112.
2. W.-T. Koo, S.-J. Choi, N.-H. Kim, J.-S. Jang and I.-D. Kim, Sensors and Actuators B: Chemical, 2016, 223, 301-310.
3. B. Behera and S. Chandra, Materials Science in Semiconductor Processing, 2018, 86, 79-84.
4. Z. Wang, M. Hu, Y. Wei, J. Liu and Y. Qin, Applied Surface Science, 2016, 362, 525-531.
5. S. S. Shendage, V. L. Patil, S. P. Patil, S. A. Vanalakar, J. L. Bhosale, J. H. Kim and P. S. Patil, Journal of Analytical and Applied Pyrolysis, 2017, 125, 9-16.
6. S. S. Shendage, V. L. Patil, S. A. Vanalakar, S. P. Patil, N. S. Harale, J. L. Bhosale, J. H. Kim and P. S. Patil, Sensors and Actuators B: Chemical, 2017, 240, 426-433.
7. B. Xiao, D. Wang, F. Wang, Q. Zhao, C. Zhai and M. Zhang, Ceramics International, 2017, 43, 8183-8189.
8. Z. Wang, D. Wang and J. Sun, Sensors and Actuators B: Chemical, 2017, 245, 828-834.
9. V. V. Ganbavle, S. V. Mohite, J. H. Kim and K. Y. Rajpure, Current Applied Physics, 2015, 15, 84-93.
10. Z. Wang, P. Sun, T. Yang, Y. Gao, X. Li, G. Lu and Y. Du, Sensors and Actuators B: Chemical, 2013, 186, 734-740.

11. J.-S. Kim, J.-W. Yoon, Y. J. Hong, Y. C. Kang, F. Abdel-Hady, A. A. Wazzan and J.-H. Lee, Sensors and Actuators B: Chemical, 2016, 229, 561-569.
12. Z. Meng, A. Fujii, T. Hashishin, N. Wada, T. Sanada, J. Tamaki, K. Kojima, H. Haneoka and T. Suzuki, Journal of Materials Chemistry C, 2015, 3, 1134-1141.
13. X. Jie, D. Zeng, J. Zhang, K. Xu, J. Wu, B. Zhu and C. Xie, Sensors and Actuators B: Chemical, 2015, 220, 201-209.
14. Parag V. Adhyapak, A. D. Bang, P. More and N. R. Munirathnam, RSC Advances, 2018, 8, 34035-34040.
15. W. Liu, L. Xu, K. Sheng, C. Chen, X. Zhou, B. Dong, X. Bai, S. Zhang, G. Lu and H. Song, Journal of Materials Chemistry A, 2018, 6, 10976-10989.
16. S. Zhao, Y. Shen, P. Zhou, X. Zhong, C. Han, Q. Zhao and D. Wei, Sensors and Actuators B: Chemical, 2019, 282, 917-926.
17. J. Qi, K. Chen, Y. Xing, H. Fan, H. Zhao, J. Yang, L. Li, B. Yan, J. Zhou, L. Guo and S. Yang, Nanoscale, 2018, 10, 7440-7450.
18. H. Zhang, Y. Wang, X. Zhu, Y. Li and W. Cai, Sensors and Actuators B: Chemical, 2019, 280, 192-200.
19. T. Li, Y. Shen, X. Zhong, S. Zhao, G. Li, B. Cui, D. Wei and K. Wei, Journal of Alloys and Compounds, 2020, 818, 152927.
20. J. Sun, L. Sun, N. Han, J. Pan, W. Liu, S. Bai, Y. Feng, R. Luo, D. Li and A. Chen, Sensors and Actuators B: Chemical, 2019, 285, 68-75.
21. Y. Shen, T. Li, X. Zhong, G. Li, A. Li, D. Wei, Y. Zhang and K. Wei, Vacuum, 2020, 172, 109036.
22. Y. Liu, Y. Li, F. Peng, Y. Lin, S. Yang, S. Zhang, H. Wang, Y. Cao and H. Yu, Applied Catalysis B: Environmental, 2019, 241, 236-245.
23. P. Bamola, A. Bhoumik, C. Dwivedi, V. Kaushik and H. Sharma, Materials Today: Proceedings, 2020, DOI: 10.1016/j.matpr.2020.01.046.
24. C. Ai, P. Xie, X. Zhang, X. Zheng, J. Li, A. Kafizas and S. Lin, ACS Sustainable Chemistry & Engineering, 2019, 7, 5274-5282.
25. T. Sun, H. Zhang, X. Wang, J. Liu, C. Xiao, S. U. Nanayakkara, J. L. Blackburn, M. V. Mirkin and E. M. Miller, Nanoscale Horizons, 2019, 4, 619-624.
26. Y. Wang, W. Cui, J. Yu, Y. Zhi, H. Li, Z. Y. Hu, X. Sang, E. J. Guo, W. Tang and Z. Wu, ACS Appl Mater Interfaces, 2019, 11, 45922-45929.
27. S. Wu, W. Wang, W. Tu, S. Yin, Y. Sheng, M. Y. Manuputty, M. Kraft and R. Xu, ACS Sustainable Chemistry &

- Engineering, 2018, 6, 14470-14479.
28. D. Edwards, N. Browne, K. M. Holsgrove, A. B. Naden, S. O. Sayedaghaee, B. Xu, S. Prosandeev, D. Wang, D. Mazumdar, M. Duchamp, A. Gupta, S. V. Kalinin, M. Arredondo, R. G. P. McQuaid, L. Bellaiche, J. M. Gregg and A. Kumar, *Nanoscale*, 2018, 10, 19638-19638.
29. Y. H. Chew, J. Y. Tang, L. J. Tan, B. W. J. Choi, L. L. Tan and S. P. Chai, *Chem Commun (Camb)*, 2019, 55, 6265-6268.
30. Y. Gao, J. Zhu, H. An, P. Yan, B. Huang, R. Chen, F. Fan and C. Li, *J Phys Chem Lett*, 2017, 8, 1419-1423.
31. Y. Min, X. Yang, D. Wang, K. Yang, S. Zheng, S. Li, H. Chen, J. Liang and F. Pan, *Catalysis Science & Technology*, 2019, 9, 6027-6036.
32. Z. Luo, A. S. Poyraz, C.-H. Kuo, R. Miao, Y. Meng, S.-Y. Chen, T. Jiang, C. Wenos and S. L. Suib, *Chemistry of Materials*, 2014, 27, 6-17.
33. M.-G. Ju, X. Wang, W. Liang, Y. Zhao and C. Li, *J. Mater. Chem. A*, 2014, 2, 17005-17014.
34. Z. Lu, Y. Li, T. Liu, G. Wang, M. Sun, Y. Jiang, H. He, Y. Wang, P. Zou, X. Wang, Q. Zhao and H. Rao, *Chemical Engineering Journal*, 2020, 389, 124417.
35. S. Dong, W. Tang, P. Hu, X. Zhao, X. Zhang, J. Han and P. Hu, *ACS Sustainable Chemistry & Engineering*, 2019, 7, 11795-11805.
36. H. B. Na, X. F. Zhang, Z. P. Deng, Y. M. Xu, L. H. Huo and S. Gao, *ACS Appl Mater Interfaces*, 2019, 11, 11627-11635.
37. H. Ren, L. Yan, M. Liu, Y. Wang, X. Liu, C. Liu, K. Liu, L. Zeng and A. Liu, *Sensors and Actuators B: Chemical*, 2019, 296, 126517.
38. D. H. Kim, J. S. Jang, W. T. Koo, S. J. Choi, H. J. Cho, M. H. Kim, S. J. Kim and I. D. Kim, *ACS Sens*, 2018, 3, 1164-1173.
39. F. Quan, J. Zhang, D. Li, Y. Zhu, Y. Wang, Y. Bu, Y. Qin, Y. Xia, S. Komarneni and D. Yang, *ACS Sustainable Chemistry & Engineering*, 2018, 6, 14911-14918.
40. Y. Xiong, C. Wang, C. Jin, Q. Sun and M. Xu, *ACS Sustainable Chemistry & Engineering*, 2018, 6, 13897-13906.
41. D. Li, Y. Sun, S. Chen, J. Yao, Y. Zhang, Y. Xia and D. Yang, *ACS Appl Mater Interfaces*, 2018, 10, 17175-17182.
42. Y. Zou, S. Chen, J. Sun, J. Liu, Y. Che, X. Liu, J. Zhang and D. Yang, *ACS Sens*, 2017, 2, 897-902.
43. F. Ma, J. Li, W. Li, N. Lin, L. Wang and J. Qiao, *Chem Sci*, 2017, 8, 800-805.
44. Q. Hao, T. Liu, J. Liu, Q. Liu, X. Jing, H. Zhang, G. Huang and J. Wang, *RSC Advances*, 2017, 7, 14192-14199.
45. S. Bai, Y. Ma, X. Shu, J. Sun, Y. Feng, R. Luo, D. Li and A. Chen, *Industrial & Engineering Chemistry Research*,

2017, 56, 2616-2623.

46. D. Dai and M. Fan, Materials Sciences and Applications, 2010, 01, 336-342.
47. W. J. Zhao, Q. X. Hu, N. N. Zhang, Y. C. Wei, Q. Zhao, Y. M. Zhang, J. B. Dong, Z. Y. Sun, B. J. Liu, L. Li and W. Hu, RSC Advances, 2017, 7, 32236-32245.
48. W. Fang, Y. Yang, H. Yu, X. Dong, T. Wang, J. Wang, Z. Liu, B. Zhao and M. Yang, RSC Advances, 2016, 6, 106880-106886.
49. N. Lu, R. H. Swan and I. Ferguson, Journal of Composite Materials, 2011, 46, 1915-1924.